Subsurface wavefields based on the Generalized Internal Multiple Imaging

Tariq Alkhalifah and Qiang Guo, King Abdullah University of science and technology (KAUST)

SUMMARY

Accessing full Green's functions between image points and the location of our recording surface is crucial to obtaining accurate subsurface wavefields and accurate images beyond the single scattering assumption. A direct approach to do so is offered by utilizing the recorded data combined with a background model. The process includes extrapolating the recorded data back in time followed by a simple interferometric crosscorrelation of the back propagated wavefield with the recorded data. This interferometric step offers the opportunity to extract subsurface Green's functions with the first order scattering forming the transmission component, and the second-order scattering becomes the leading scattering term. A crosscorrelation of the resulting, assumed upgoing, wavefield with a forward modeled down going wavefield highlights the double scattered reflectivity in a process referred to as the generalized internal multiple imaging (GIMI). The resulting image is vulnerable to crosstalk between different order multiples interacting with each other. Thus, we develop the adjoint GIMI that takes us from image to data, and use it to formulate a least square optimization problem to fit the image to the data. The result is reduced crosstalk and cleaner higher resolution multiple scattering images. We also extract space extensions of the image, which offers the opportunity to evaluate the focussing capability of the velocity model, and formulate updates for that model based on double scattering.

INTRODUCTION

Recorded multiple scattered energy can be invaluable in illuminating interfaces not captured by the single-scattered wavefields, which we often use in classic imaging. The multiples often appear in our images as artifacts and noise that we strive to mute, and we end up with reflections illuminated by the single scattering assumption. Multi scattered energy not only provides additional scattering information, but also it can provide additional wave information in its unique path (Alkhalifah and Wu, 2016). Using the Marchenko algorithm, an iterative imaging procedure has been suggested by Behura et al. (2012) to image all internal scatterings including the single-scattering energy. This iterative procedure does not allow for separate imaging of different orders of multiples and it also requires manual muting of anticausal events after crosscorelation. This makes their method very involved (van der Neut et al., 2015). Other developments in imaging multiple scattering are given by Malcolm et al. (2011), which image prismatic waves and other higher-order internal scatterings. Alternatively, (Malcolm et al., 2009). Zuberi and Alkhalifah (2014b) proposed to directly work with the Born series, i.e., they do not make any assumptions about the geometry of the velocity perturbations. Their approach, referred to as the Generalized Internal Multiple Imaging (GIMI) process, images any order internal scattering, separately. The GIMI process relies solely on the background Green's function based on a smooth velocity model, which we often use in imaging. The additional computational cost in GIMI is an interferometric cross-correlation of the surface seismic data with the back propagated data. The number of cross-correlations required is one less than the order of the term in the Born scattering series (or equal to the order of internal multiple) we intend to image. However, GIMI is hampered by crosstalk, and beholden to the weak scattering assumption. The crosstalk is the result of additional cross-correlations of events that are not related to each other. The small velocity perturbation assumption was, however, necessary for the convergence of the Born scattering series.

In this study, we try to mitigate GIMI's limitations by formulating a GIMI based least square optimization in which we fit the different-order multiple images to the data. To do so, we derive the adjoint GIMI operation that takes us from the image to the data. In the process of doing so, we analyze the different steps of the GIMI procedure, and suggest additional applications for some of the features we highlight. Such analysis will be demonstrated on a simple model to help us understand the process. More complicated applications including real data will be shared in the presentation of the work at the meeting.

THE IMAGING

Our objective in this section is to review the generalized internal multiple imaging (GIMI) process and highlight some of its features with a simple model example. The model is made up of two homogeneous layers, as shown in Figure 1a, with a vertical reflector that can not be captured with single scattering imaging. This model is representative of a fault or a Salt flank, and is sampled at 0.01524 km in both directions requiring 200 samples laterally and 100 vertically. The velocity of the first layer is 2.4 km/s and the second layer 2.7 km/s. Using a Ricker wavelet with peak frequency 18Hz, we generate synthetic data using a finite-difference scheme for an acoustic isotropic constant-density medium. The data correspond to 21 shots and 100 receivers both equally sampled to cover the surface area of the model. Figure 1b shows a representative shot gather for a source located 2.286 km, as shown in Figure 1a. The later reflection on the right side of the section corresponds to double scattering from the vertical reflector.

10.1190/segam2018-2997637.1

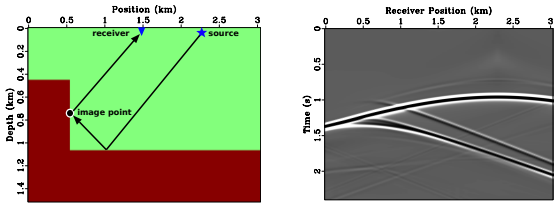

(a) (b)

Figure 1: a) The velocity model with an example double-bounce raypath that could image the vertical reflector. The image point location will be used to analyze the GIMI procedure. b) A shot gather corresponding to the shot point location in a).

The GIMI process is capable of imaging internal multiples of any order. The key is an interferometric step that translates the energy from higher-order scattering to become a leading scattering term. The main requirement is that the sources and receivers cover the same surface, preferably sampled well. Thus, as introduced by Zuberi and Alkhalifah (2014a), the GIMI process to image double scattered energy includes three steps:

1. Back propagate the recorded data from the surface to the model points.
2. An interferometric crosscorrelation of the back propagated wavefield with the recorded data over sources.
3. Zero-lag crosscorrelation of the interferometric data with modeled data from the surface.

The result is a function of the medium containing reflectively corresponding mostly to double-bounce events. It also contains artifacts caused by higher order scattering (crosstalk) and low frequency energy corresponding to the first-order scattering. The key step here is the middle interferometric step. The other steps are similar to what we do for the single scattering imaging process, like reverse time migration (RTM). A repeat of the interferometric crosscorrelation between the output from step 2 and the data on the recording surface over receivers highlights triple scattering as the leading scattering term.

To demonstrate the physical meaning of these operations, we track the evolution of wavefields after every step of GIMI. In the imaging process we use the velocity of the first layer (2.4 km/s). In mathematical terms, we can write the three steps, constituting GIMI, in three equations starting with the conventional back propagation of the recorded reflections corresponding to up going wavefields, $\mathbf{R}^-$ (a shot representation is given in Figure 1b), to obtain the mainly upgoing wavefield (superscript -) from the source, $\mathbf{s}$, to the point, $\mathbf{x}$:

$$\mathbf{G^-_{xs}} = \mathbf{G^b_{rx}}^* \mathbf{R^-_{rs}}, \tag{1}$$

with the Einstein summation notation used over r, and $\mathbf{G^b_{rx}}^*$ is the complex conjugate (superscript *) of the background Green's function from $\mathbf{x}$ to $\mathbf{r}$. This is equivalent to the first step of reverse time migration. Figure 2a shows such wavefields for the image point shown in Figure 1a as a function of sources and time. The resulting wavefield $\mathbf{G^-_{xs}}$ is not purely upgoing as it contains even down going waves and other events, but what we care for, and try to isolate, the double scattering, is upgoing. In the Marchenko process, with an opposite side implementation (source side), the directionality of the waves are identified using the causal and anti causal parts of the correlation process along with muting in an iterative process (van der Neut et al., 2015). Here, we will try to make things simple. Thus, we next perform the interferometric step given by

$$\mathbf{G^-_{rx}} = \mathbf{R^-_{rs}} \mathbf{G^-_{xs}}^*, \tag{2}$$

with the Einstein summation notation, which constitutes a summation over sources here. This step, as described by Zuberi and Alkhalifah (2014a), moves the second-order scattering term to be the leading scattering term heading in the upward direction (thus, the negative sign in $\mathbf{G^-_{rx}}$). Meanwhile, the first-order scattering term will be propagating downward, like those we experience with diving waves. Figure 2b shows the result of this step for the same image point shown in Figure 1a, but now as a function of receivers and time. The corresponding background down going wavefield, $(\mathbf{G^b_{rx}})^+$, is shown in Figure 2c. Finally, the imaging condition for double scattering:

$$\mathbf{I_x} = (\mathbf{G^b_{rx}})^{+^*} \mathbf{G^-_{rx}}, \tag{3}$$

which includes a summation over receivers. The result is an image of the second-order scattering as a leading term of the scattering series, marred with low frequency wave path energy between the recording surface and the reflectors, as shown in Figure 3a. These wavepath low-wavenumber components of the image can be removed in many ways, including using a Laplace filter, separating up and down going wavefields prior to crosscorrelation, or some innovative imaging conditions, like the inverse scattering imaging condition (Whitmore and Crawley, 2012). We use a simple 2D low-cut filter to obtain Figure 3b, which highlights the double scattering reflectivity.

To obtain higher-order scattering images, the middle step in GIMI is replaced by:

$$\mathbf{G^-_{rx}} = \left[\mathbf{R^-_{es}} \mathbf{G^-_{xs}}^*\right]^* \mathbf{R^-_{re}}, \tag{4}$$

which will highlight triple scattering. For fourth-order scattering:

$$\mathbf{G^-_{rx}} = \mathbf{R^-_{rv}} \left[\left[\mathbf{R^-_{es}} \mathbf{G^-_{xs}}^*\right]^* \mathbf{R^-_{ve}}\right]^*, \tag{5}$$

and so on. Figure 3c shows the image for triple scattering, and mainly it highlights the double scattering

10.1190/segam2018-2997637.1

wavepaths. A similar filter to that used for double scattering is applied here to obtain the image in Figure 3d. The sharp edges of the model includes triple scattering.

The only weakness in this direct process for imaging is the crosstalk as the upgoing wavefield $\mathbf{G}^-_{\mathbf{xs}}$ is not purely upgoing and contains additional events. In fact, if we look closely to Figure 3b, we realize that we have some artifacts and the resolution is low, both of which we hope to resolve using a least square optimization. The low resolution is also attributable to the coarse shot sampling used in this demonstration.

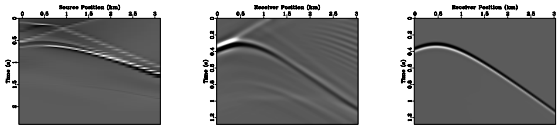

(a) (b) (c)

Figure 2: a) The function $\mathbf{G}^-_{\mathbf{xs}}$; b) The function $\mathbf{G}^-_{\mathbf{rx}}$; c) The function $(\mathbf{G}^{\mathbf{b}}_{\mathbf{rx}})^+$. All three functions plotted for the image point in Figure 1a.

THE ADJOINT

We, next, formulate the adjoint of the generalized internal multiple imaging (GIMI) to use in a least square implementation to reduce the crosstalk artifacts associated with the process. As GIMI transforms the full recorded data to an image corresponding to double scattering (or higher-order scattering). The adjoint operation should produce the approximate full recorded upgoing data from the double scattered image.

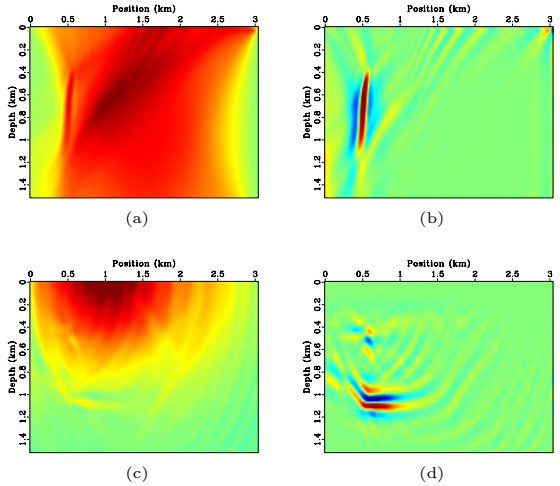

(a) (b) (c) (d)

Figure 3: a) The image $\mathbf{I_x}$; b) The image $\mathbf{I_x}$ after a low cut filter; c) The triple scattering image, d) and the filter.

An adjoint operation can be formulated by recognizing that the interferometric step remains the same. Since the other two steps of GIMI constitute single scattering imaging, the adjoint is mainly given by Born scattering. Thus, for the adjoint, we have the following three steps:

$$\mathbf{G}^-_{\mathbf{xs}} = \mathbf{I_x}(\mathbf{G}^{\mathbf{b}}_{\mathbf{xs}})^+, \tag{6}$$

which isolates the source wavefield at the image locations, and we care mainly for the part heading upward as it is scattered. In classic Born scattering (or more accurately demigration), $G^-_{x\,s}$ is the source of the scattered wavefield so we convolve it with a Green's function from the image point to the surface, $G_{r\,x}$ ($\mathbf{R}^-_{\mathbf{rs}} = (G^b_{r\,x})^- G^-_{x\,s}$). Since the image pertains to double scattering, we first pass $\mathbf{G}^-_{\mathbf{xs}}$ through the interferometric step:

$$\mathbf{G}^-_{\mathbf{rx}} = \mathbf{R}^-_{\mathbf{rs}} \mathbf{G}^{-\,*}_{\mathbf{xs}}, \tag{7}$$

Finally, we convolve it with the background Green's function from the source to the image point:

$$\mathbf{R}^-_{\mathbf{rs}} = \mathbf{G}^-_{\mathbf{rx}}(\mathbf{G}^{\mathbf{b}}_{\mathbf{xs}})^+, \tag{8}$$

which is the forward propagation of $\mathbf{G}^-_{\mathbf{rx}}$ from $\mathbf{x}$ to $\mathbf{s}$, relying on reciprocity theory. Figure 4a shows the modeled data from the double scattering image shown in Figure 3a. Note that the adjoint will approximately reproduce the full data, even through the image corresponds to mainly the double scattering, as the single scattering resides in the wavepath parts of the image. If we modeled the filtered image in Figure 3b, we obtain data corresponding mainly to the double scattering term.

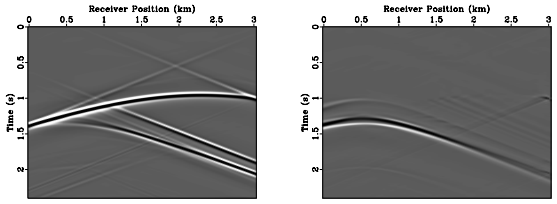

(a) (b)

Figure 4: a) The modeled data from the double scattered image in Figure 3a for the shot location shown in 1a; b) Same as a) starting from the filtered image in Figure 3b. In both cases, the constant velocity of the first layer was used for modeling.

THE LEAST SQUARE IMPLEMENTATION

Since we have the imaging operation and its adjoint, we can formulate a least square optimization problem to find the second-order scattering image that fits the data. We can also utilize additional regularization terms to improve such an image (i.e. in resolution (Aldawood et al., 2015, 2016)).

10.1190/segam2018-2997637.1

An optimization problem can be formulated to improve the image with an objective function:

$$J(\mathbf{I_x}) = |\mathbf{R^-_{rs}} - \mathbf{R^m_{rs}}(\mathbf{I_x})|^2_2, \tag{9}$$

such that $\mathbf{R^m_{rs}}(\mathbf{I_x})$ is the modeled reflections from the double scattering image $\mathbf{I_x}$ using equations 6- 8. The operation $|.|^2_2$ stands for the l_2 norm. The gradient is given by the adjoint applied to the residual $\mathbf{\Delta R} = \mathbf{R^-_{rs}} - \mathbf{R^m_{rs}}(\mathbf{I_x})$ using equations 1- 3. Initially, we set $\mathbf{I_x} = 0$, and thus, $\mathbf{\Delta R} = \mathbf{R^-_{rs}}$, and the image is given by GIMI, and shown in Figure 3b. We, then, use this image to compute $\mathbf{R^m_{rs}}(\mathbf{I_x})$ shown in Figure 3b. The difference between $\mathbf{R^m_{rs}}(\mathbf{I_x})$ and the data form the residuals, used as the adjoint source to update the image. Like conventional least square migration, we continue the iterative process until we meet a convergence criterion. After 20 iterations, we obtain the image shown Figure 5. It is free of artifacts and has higher resolution compared to Figure 3b.

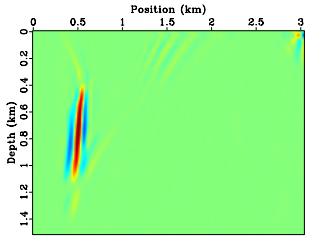

Figure 5: The least square image.

SPACE EXTENSIONS

The multi-scattering image can, like the single scattering case, be used to evaluate the accuracy of the velocity model, by assessing the focussing of energy to zero lag when we introduce an extension. Introducing an extension to GIMI, implies we need to compare up and down going wavefields at points that are not coincident, and specifically located $2\mathbf{h}$ apart, where $\mathbf{h}$ is the subsurface space extension. The offset between these points formulates the subsurface offset, and provides data (or images) corresponding to subsurface sources and receivers that are not coincident (Vasconcelos et al., 2010). Conveniently, the extensions are introduced to GIMI in the last step:

$$\mathbf{I_{x\,h}} = \mathbf{G^b_{r\,x+h}}^{+*}\mathbf{G^-_{r\,x-h}}, \tag{10}$$

Alternatively,

$$\mathbf{I_{s'\,r'}} = \mathbf{G^b_{r\,s'}}^{+*}\mathbf{G^-_{r\,r'}}, \tag{11}$$

where $\mathbf{s'}$ and $\mathbf{r'}$ are indexes corresponding to the locations of the subsurface source and receiver, respectively. In both cases, if the velocity is accurate, we expect the energy to be focussed at $\mathbf{h} = 0$ or $\mathbf{s'} = \mathbf{r'}$. Applying a multi dimensional extension is costly. Since horizontal layering dominate our data, we often utilize a horizontal extension. Such an extension provides the necessary information to evaluate the velocity model for a layered medium. If the reflector of interest is vertical, we will need a vertical extension as horizontal extensions are, in this case, not dependent on the velocity. For the example model shown in Figure 1a, the reflector of interest is vertical, and thus, velocity sensitivity is expected to show in the vertical extension. Figure 6 shows the extension vertically, h_z, for the area containing the vertical reflector. We repeat the GIMI with an inaccurate velocity of the first layer, and as a result, some energy is not focussed at zero lag. Such non-focussing has distinct features for lower and higher velocities. Using the adjoint, we can utilize such energy to update the velocity along the path of the double scattering.

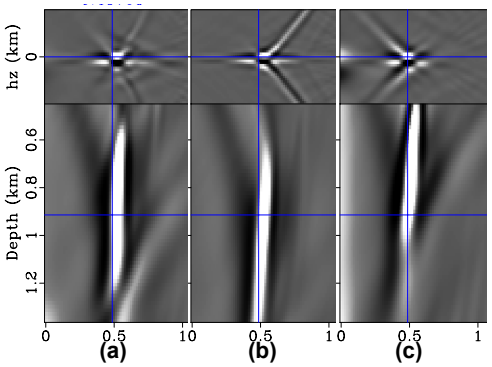

Figure 6: a) The extended image horizontally (top, h_z) in the area around the vertical reflector shown in Figure 3a; b) The same extensions using a lower (2.1 km/s) than the first layer (2.4 km/s) velocity in GIMI; c) The same extensions using a higher (2.7 km/s) than the first layer velocity in GIMI.

CONCLUSION

We developed the adjoint operation to the generalized internal multiple imaging (GIMI). Since GIMI is susceptible to cross talk and resolution issues, using the adjoint we formulated a least square optimization problem to invert for the image. The interferometric crosscorrelation step in GIMI converts the leading scattering term to a transmission component, which can be suppressed using a Laplacian filter or any advanced imaging condition. More importantly, it transforms second-order scattering to be the leading scattering term, which results in images corresponding to double scattering. Higher-order scattering is attained by additional interferometric correlations. Space extensions of the double scattering image can be used to evaluate the focussing and the velocity model used in GIMI.

ACKNOWLEDGMENTS

We thank KAUST for its support. We thank the SWAG group including Mohammad Zuberi for useful discussions. We also thank Ivan Vasconcelos for fruitful exchanges.

10.1190/segam2018-2997637.1

REFERENCES

Aldawood, A., I. Hoteit, and T. Alkhalifah, 2016, The linearized inversion of the generalized interferometric multiple imaging: 86th Annual International Meeting, SEG, Expanded Abstracts, 4250–4254, https://doi.org/10.1190/segam2016-13680101.1.

Aldawood, A., I. Hoteit, M. Zuberi, G. Turkiyyah, and T. AlKhalifah, 2015, The possibilities of least- squares migration of internally scattered seismic energy: Geophysics, **80**, no. 4, S93–S101, https://doi.org/10.1190/geo2014-0436.1.

Alkhalifah, T., and Z. Wu, 2016, Multiscattering inversion for low-model wavenumbers: Geophysics, **81**, no. 6, R417–R428, https://doi.org/10.1190/geo2015-0650.1.

Behura, J., K. Wapenaar, and R. Snieder, 2012, Newton-Marchenko-Rose imaging: SEG, 1–6.

Malcolm, A., M. De Hoop, and B. Ursin, 2011, Recursive imaging with multiply scattered waves using partial image regularization: A north sea case study: Geophysics, **76**, no. 2, B33–B42, https://doi.org/10.1190/1.3537822.

Malcolm, A. E., B. Ursin, and M. V. De Hoop, 2009, Seismic imaging and illumination with internal multiples: Geophysical Journal International, **176**, 847–864, https://doi.org/10.1111/gji.2009.176.issue-3.

van der Neut, J., I. Vasconcelos, and K. Wapenaar, 2015, On green's function retrieval by iterative substitution of the coupled Marchenko equations: Geophysical Journal International, **203**, 792–813, https://doi.org/10.1093/gji/ggv330.

Vasconcelos, I., P. Sava, and H. Douma, 2010, Nonlinear extended images via image-domain interferometry: Geophysics, **75**, no. 6, SA105–SA115, https://doi.org/10.1190/1.3494083.

Whitmore, N. D., and S. Crawley, 2012, Applications of RTM inverse scattering imaging conditions: 82th Annual International Meeting, SEG, Expanded Abstracts, 1–6, https://doi.org/10.1190/segam2012-0779.1.

Zuberi, M. A. H., and T. Alkhalifah, 2014a, Generalized internal multiple imaging: Geophysics, **79**, no. 5, S207–S216, https://doi.org/10.1190/geo2013-0287.1.

Zuberi, M. A. H., and T. Alkhalifah, 2014b, Generalized internal multiple imaging (GIMI) using feynman-like diagrams: Geophysical Journal International, **197**, 1582–1592, https://doi.org/10.1093/gji/ggt527.